Journal of Magnetic Resonance Open 16–17 (2023) 100129

Contents lists available at ScienceDirect

Journal of Magnetic Resonance Open

journal homepage: www.sciencedirect.com/journal/journal-of-magnetic-resonance-open

Facile hyperpolarization chemistry for molecular imaging and metabolic tracking of [1–^{13}C]pyruvate in vivo

Keilian MacCulloch [a,1], Austin Browning [a,1], David O. Guarin Bedoya [b], Stephen J. McBride [a], Mustapha B. Abdulmojeed [a], Carlos Dedesma [c], Boyd M. Goodson [d], Matthew S. Rosen [b], Eduard Y. Chekmenev [e,f], Yi-Fen Yen [b], Patrick TomHon [c,*], Thomas Theis [a,g,h,*]

[a] Department of Chemistry, North Carolina State University, Raleigh, NC, 27695,United States of America
[b] Department of Radiology, Athinoula A. Martinos Center for Biomedical Imaging, Massachusetts General Hospital, Charlestown, MA, United States of America
[c] Vizma Life Sciences Inc., Chapel Hill, NC, 27514, United States
[d] School of Chemical & Biomolecular Sciences and Materials Technology Center, Southern Illinois University, Carbondale, IL, 62901, United States of America
[e] Department of Chemistry, Integrative Bio-sciences (Ibio), Karmanos Cancer Institute (KCI), Wayne State University, Detroit, MI, 48202, United States of America
[f] Russian Academy of Sciences, 119991, Moscow, Russia
[g] Department of Physics, North Carolina State University, Raleigh, NC, 27606, United States of America
[h] Joint UNC & NC State Department of Biomedical Engineering, North Carolina State University, Raleigh, NC, 27606, United States of America

ARTICLE INFO

Keywords:
Hyperpolarized MRI
Parahydrogen
SABRE
Metabolic imaging

ABSTRACT

Hyperpolarization chemistry based on reversible exchange of parahydrogen, also known as Signal Amplification By Reversible Exchange (SABRE), is a particularly simple approach to attain high levels of nuclear spin hyperpolarization, which can enhance NMR and MRI signals by many orders of magnitude. SABRE has received significant attention in the scientific community since its inception because of its relative experimental simplicity and its broad applicability to a wide range of molecules, however, *in vivo* detection of molecular probes hyperpolarized by SABRE has remained elusive. Here we describe a first demonstration of SABRE-hyperpolarized contrast detected *in vivo*, specifically using hyperpolarized [1–^{13}C]pyruvate. Biocompatible formulations of hyperpolarized [1–^{13}C]pyruvate in, both, methanol-water, and ethanol-water mixtures followed by dilution with saline and catalyst filtration were prepared and injected into healthy Sprague Dawley and Wistar rats. Effective hyperpolarization-catalyst removal was performed with silica filters without major losses in hyperpolarization. Metabolic conversion of pyruvate to lactate, alanine, and bicarbonate was detected *in vivo*. Pyruvate-hydrate was also observed as a minor byproduct. Measurements were performed on the liver and kidney at 4.7 T via time-resolved spectroscopy and chemical-shift-resolved MRI. In addition, whole-body metabolic measurements were obtained using a cryogen-free 1.5 T MRI system, illustrating the utility of combining lower-cost MRI systems with simple, low-cost hyperpolarization chemistry to develop safe and scalable molecular imaging.

Introduction

Traditional NMR and MRI approaches, which rely on thermal nuclear spin polarization, face significant sensitivity limitations compared to other analytical chemistry or medical imaging techniques, and require relatively high concentrations of detected molecules. To address the sensitivity challenge faced by MR approaches, hyperpolarization methods have been developed to align much larger fractions of nuclear spins and to improve the sensitivity limits of NMR and MRI by several orders of magnitude[1–6]. Indeed, the first hyperpolarized (HP) contrast agent (^{129}Xe gas)[7–11] has been FDA approved for ventilation lung imaging. Other HP molecular probes are also emerging for molecular imaging, including [1–^{13}C]pyruvate[12]. HP [1–^{13}C]pyruvate is similar to the [^{18}F]fluorodeoxyglucose PET[13,14] tracer in that it allows molecular sensing of aberrant energy pathways in cancer[2,3] and many other diseases[15,16]. Currently in over 30 clinical trials, dissolution

Abbreviations: NMR, Nuclear Magnetic Resonance; MRI, Magnetic Resonance Imaging; SABRE, Signal Amplification By Reversible Exchange; HP, Hyperpolarized; PET, Positron Emission Tomography; D-DNP, dissolution Dynamic Nuclear Polarization.

* Corresponding authors.
E-mail addresses: patrick@vizma.ai (P. TomHon), ttheis@ncsu.edu (T. Theis).

[1] These authors contributed equally.

https://doi.org/10.1016/j.jmro.2023.100129

Available online 13 July 2023

Dynamic Nuclear Polarization (D-DNP)[17] is the hyperpolarization method employed for production of HP [1–^{13}C]pyruvate for molecular imaging applications. Hyperpolarized MRI can directly track and image metabolic events at any depth inside tissue at modest sub-mM concentrations and it is relatively safe because HP MRI uses injectable contrast agents that are endogenous biomolecules, instead of radioactive material. The disadvantages of D-DNP are that it is infrastructure-intensive and relatively slow to build up hyperpolarization (~1 hour). A faster and perhaps simpler approach to hyperpolarize [1–^{13}C]pyruvate is parahydrogen-induced polarization (PHIP)[5,18-20]. One possibility is side-arm hydrogenation PHIP (SAH-PHIP)[21,22], which has been successfully used to hyperpolarize [1–^{13}C]pyruvate[23–25], the most common hyperpolarized MRI tracer. In SAH-PHIP an unsaturated side arm of a pyruvate ester is hydrogenated with parahydrogen, the polarization is transferred to the ^{13}C nucleus, and the pyruvate is then cleaved via hydrolysis of the ester. Although SAH-PHIP is a successful approach for PHIP hyperpolarization of [1–^{13}C]pyruvate, the synthesis of the unsaturated pyruvate ester precursors is relatively complex and storage is not trivial. Unlike any existing method, Signal Amplification By Reversible Exchange (SABRE) hyperpolarizes sodium [1–^{13}C]pyruvate directly and without the need for chemical modifications[26,27]. As depicted in Fig. 1, SABRE relies on reversible exchange of parahydrogen and a to-be-hyperpolarized substrate, [1–^{13}C]pyruvate in the present case, on an Ir-catalyst to create a spin network connecting parahydrogen and the target substrate. Continuous reversible exchange of parahydrogen and the substrate leads to rapid polarization build-up within the bulk [1–^{13}C]pyruvate molecules in solution. In principle, the resulting HP agent can be processed to quickly obtain biocompatibility for subsequent injection into the subject to monitor metabolic changes.

Since its inception[26–28], SABRE hyperpolarization chemistry has undergone significant developments[29–32]. First, SABRE was primarily optimized to hyperpolarize protons in target substrates[26-28,33]. With the invention of the SABRE-SHEATH (SABRE in Shield Enables Alignment Transfer to Heteronuclei) variant, it became possible to efficiently hyperpolarize ^{15}N and ^{13}C nuclei that are associated with longer hyperpolarization lifetimes[34–42]—such as in [1–^{13}C]pyruvate [43,44]. Subsequent developments enabled polarization levels exceeding 10% using temperature cycling[45,46] and/or various pulsed-field approaches[47–50]. Building on these recent advances, here we show the first detection of a SABRE-hyperpolarized substrate, [1–^{13}C]pyruvate, *in vivo*. Using a rat model, spectroscopic tracking of metabolic turnover and Chemical Shift Imaging (CSI) are demonstrated for kidney, liver, and whole body at multiple experimental sites, pointing towards the development of a truly scalable molecular imaging technique resulting from the combination of fast, simple SABRE hyperpolarization chemistry with low-cost, cryogen-free MRI[51–55].

Methods

Sample preparation

Under inert gas conditions, [1–^{13}C]pyruvate, [Ir(IMes)(COD)Cl] (IMes= 1,3 bis(2,4,6-trimethylphenyl)imidazole-2-ylidene, COD=cyclooctadiene) polarization-transfer pre-catalyst, and DMSO were mixed to give absolute concentrations of 65 mM [1–^{13}C]pyruvate, 24 mM DMSO, and 6 mM Ir-IMes in CD_3OD. Ir-IMes catalyst was synthesized using literature methods[56,57]. Dry CD_3OD was used as provided from the supplier (Cambridge Isotopes) and degassed with 5 freeze-pump-thaw cycles. All other chemicals used were purchased from Millipore Sigma.

Hyperpolarization and sample processing

[1–^{13}C]pyruvate was hyperpolarized by bubbling parahydrogen through a 500 μL solution containing 6 mM iridium-IMes catalyst, 24 mM DMSO, and 65 mM [1–^{13}C]pyruvate at 100 psi inside a standard NMR tube using a previously described bubbling setup[46]. The sample is pre-cooled to 0 °C and then, as illustrated in Fig. 2, placed into a Polarization Transfer Field (PTF) of 0.3 μT established in mu-metal shields provided by MagneticShield Corp. (ZG-203). After 90 s of bubbling parahydrogen, at room temperature and 0.3 μT field, hyperpolarization of about 10% is achieved, and the sample is manually transferred into a 0.3 T Halbach array, where the parahydrogen pressure is released. The sample is subsequently pulled into a syringe prefilled with saline solution, creating a saline-methanol mixture. For the experiments at 4.7 T at Massachusetts General Hospital (MGH), 1.5 mL saline was used creating at total injectable volume of 2 mL, with a methanol-to-saline ratio of 1:3. These concentrations correspond to a pyruvate dosage of 11.3 mg/kg (0.13 mmol/kg) injected into ~250 g Sprague Dawley rats. For the experiments at 1.5 T (at NC State) using the cryogen-free MRI system, only 1 mL of saline was used, creating a total injectable volume of 1.5 mL with a methanol-to-saline ratio of 1:2. These concentrations correspond to a pyruvate dosage of 14.1 mg/kg (0.16 mmol/kg) injected into ~200 g Wistar rats. These dosages of hyperpolarized and injected pyruvate are lower than those in typical D-DNP hyperpolarized MRI studies, which are closer to (0.75 to 1 mmol/kg) [58–62]. For all animal studies, the rats were sedated with isoflurane before placing them in the MRI scanner. Isoflurane was continuously provided via a nose cone in the MRI scanner during experimentation, and the heart and breathing rates were continuously monitored. The vitals remained stable after injection, and the animals were euthanized before waking from anaesthesia, approximately 10 min after completion of the experiment. While the injected quantities of methanol in these proof-of-concept studies were near the LD50, the toxic effects of methanol are delayed well past the timepoint of euthanasia, allowing the described experiments. All animal handling procedures were conducted under the appropriate IACUC protocols at NC State and MGH. At NC

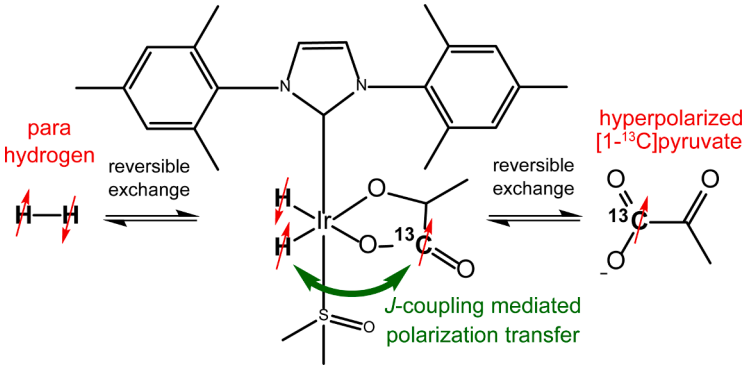

Fig. 1. SABRE hyperpolarization chemistry: both parahydrogen and the [1–^{13}C]pyruvate substrate are in reversible exchange with the polarization transfer catalyst, [IrH_2(IMes)(DMSO)(pyruvate)]. During the lifetime of the polarization-transfer complex, comprising the catalyst, substrate, and parahydrogen (tens to hundreds of milliseconds), the polarization is transferred from the parahydrogen singlet state on the hydrides to the ^{13}C nucleus in pyruvate transiently bound on the catalyst. Continuous exchange leads to hyperpolarization build-up on the free pyruvate in solution. This build-up process requires roughly 1.5 min to reach steady-state hyperpolarization.

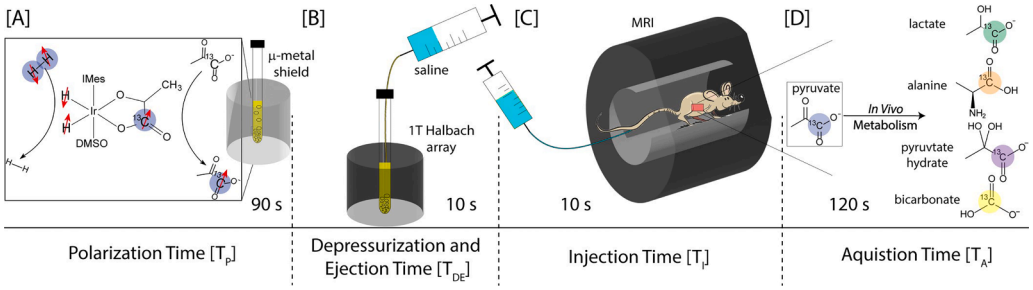

Fig. 2. Experimental procedure of MRI *in vivo* studies. [A] SABRE hyperpolarization takes place inside of a mumagnetic shield at a polarization transfer field of 0.3 μT. The sample is precooled to 0 °C and then parahydrogen is bubbled through the solution for 90 s allowing for polarization buildup in the magnetic shields. [B] The sample is transferred to a 0.3 T Halbach array (to help slow relaxation of the hyperpolarization) for depressurization and ejection into a syringe pre-filled with saline, taking 10 s. [C] After ejection the sample is moved across the room and attached to the catheter for injection, requiring ~10 s. [D] After injection, a two-minute scan is applied with 20° pulses and repetition time of 2 s to detect the metabolic products of pyruvate—namely lactate, alanine, and bicarbonate. (Pyruvate-hydrate is also detected).

State, hyperpolarized ^{13}C MR data were acquired from the whole body of the animals. The cryogen-free, variable-field MRI system at NC State used whole body transmit/receive ^{13}C volume coils (5.2 cm RF window length and 6.5 cm in diameter). The spectroscopic data were obtained using 20° non-selective 0.314 ms hard pulses, a repetition time (TR) of 2 s including a 0.68 s acquisition time, 12 kHz spectral bandwidth, and 8192 spectral points.

At MGH, the hyperpolarized ^{13}C animal experiment was conducted on a 4.7 T animal MRI scanner (Bruker Biospin, Billerica, USA) using a commercial transmit/receive proton volume coil (Bruker, Billerica, USA) for localization and shimming. ^{13}C experiments used a custom-made transmit/receive ^{13}C surface coil with a 6 cm inner diameter for ^{13}C acquisitions. In the dynamic spectroscopy experiments, a pulse-and-acquire sequence was used with a non-selective 0.11 ms hard pulse, centred at 180 ppm with a 30° nominal flip angle and a repetition time (TR) of 3 s. For all chemical shift imaging (CSI) experiments, a sinc pulse with 11,000 Hz bandwidth and 0.56 ms length was used to selectively excite a single axial slice of 15 mm thickness. CSI parameters were: TR 410 ms, echo time (TE) 1.05 ms, 20° nominal flip angle, spectral bandwidth 10,080 Hz, 4096 spectral points, field of view (FOV) of 80 mm × 40 mm, and matrix size 8 × 8. Fig. 2 provides a general overview of the experimental procedures.

Results and discussion

In vivo spectroscopy at 4.7 T

Fig. 3 shows the data obtained for the first observation of metabolic conversion using dynamic spectroscopy employing SABRE-hyperpolarized [1–^{13}C]pyruvate. The surface coil was placed either on the liver or the kidney of the rat, the hyperpolarization was started, followed by dilution with saline, injection, and data acquisition. As seen in Fig. 3, the data clearly show peaks for lactate, alanine, pyruvate-hydrate, and bicarbonate. Figs. 3A-C show the data acquired from the liver, and Figs. 3D-F from the kidney. In comparison, the data from the liver clearly shows a higher metabolic rate as expected[58], while noting that in the presented pilot studies significant quantities of methanol were injected, which is known to alter metabolism[63,64]. Future work will use ethanol/water as described below, or fully aqueous injectables [65]. Figs. 3A and D show spectra created by summing the data across the full time duration for liver and kidney, respectively. Most metabolic turnover is observed to lactate and alanine, whereas conversion to pyruvate-hydrate and bicarbonate is less pronounced. Figs. 3B and E show the full time-resolved spectra. Figs. 3C and F show the corresponding projection of the signals for pyruvate, lactate, and alanine as a function of time, revealing the time course of pyruvate perfusion convoluted with metabolic conversion and T_1 relaxation for the individual metabolites—as expected from previous D-DNP work[58]. As can be seen, metabolic tracking for about one minute was possible in these first proof-of-concept studies.

In vivo spectroscopic imaging at 4.7 T

In addition to *in vivo* spectroscopy, we implemented Chemical Shift Imaging (CSI) to visualize the spatial distribution of the SABRE-hyperpolarized [1–^{13}C]pyruvate within the kidney and liver as displayed in Fig. 4. The individual spectra were integrated and turned into a heat map superimposed on an anatomical proton-MRI slice of the

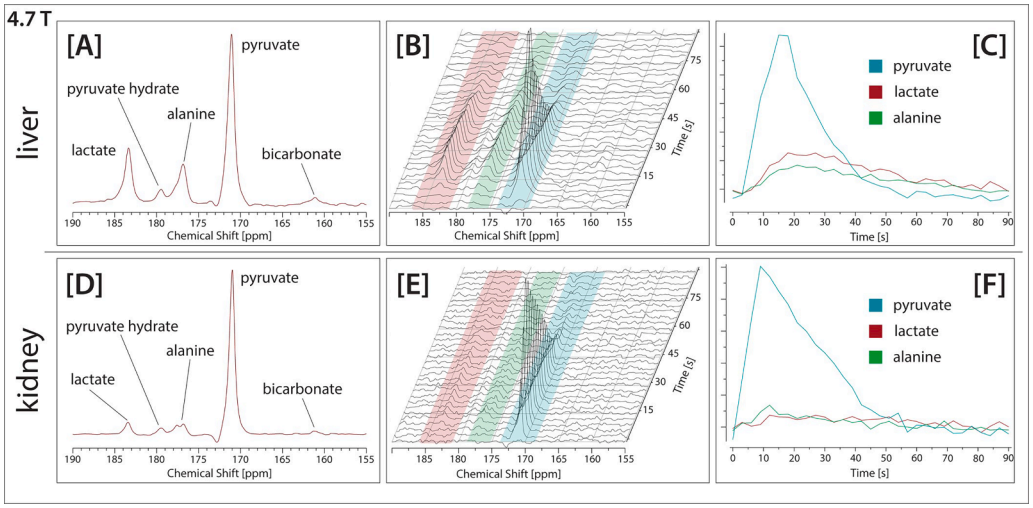

Fig. 3. *In vivo* spectra acquired on two rats (Sprague Dawley, female) using a dynamic spectroscopy sequence and a different field of view on the liver [A-C] and kidney [D-F]. [A, D] Summed spectra of the complete dynamic spectroscopy acquisition. [B, E] Spectra overlay of the dynamic-spectroscopy acquisition with lactate (red), alanine (green), and pyruvate (blue) integration regions highlighted. [C, F] Plot of the integrated acquisition for pyruvate, lactate, and alanine using the spectra shown in B and E. The spectra in this temporal series are acquired with 30° flip angle and 3 s delay between acquisitions.

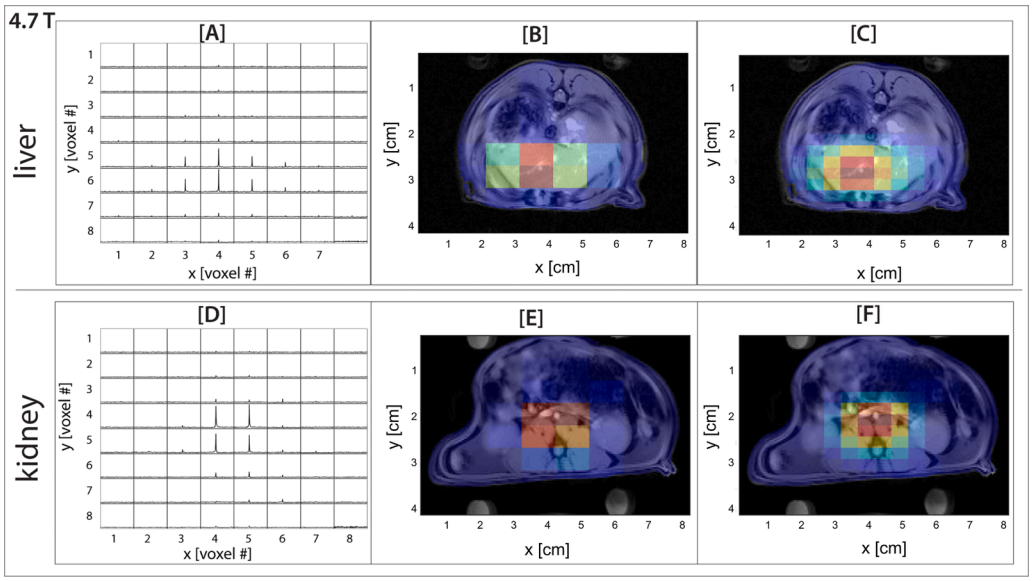

Fig. 4. Chemical Shift Imaging (CSI) experiments on two separate animals (shown in separate rows) with two different fields of view (liver, row 1; kidney, row 2). [A, D] 8 × 8 array of the 64 spectra acquired in the respective CSI experiments. [B, E] Integration of the peaks shown in the spectra to obtain a intensity map overlayed on top of the centre anatomical slice of the imaged region. [C, F] zero-filled intensity map (16 × 16) for visualization of the CSI results. CSI results are acquired linearly in a 8 × 8 matrix using a 20° flip angle and a 0.41 s TR.

imaged region. Figs. 4A-C show the data acquired with the surface coil placed on the liver, whereas Figs. 4D-E show the data acquired when the surface coil was placed on the kidney. Figs. 4A and D show the respective raw CSI data displaying the spectra acquired in a 8 × 8 grid covering a field of view (FOV) of 8 × 4 cm^2. Figs. 4B and E each show a heatmap over the corresponding anatomical image, which was then smoothed by zero-filling the data to assist with visualization—as shown in Figs. 4C and F. In this work, the excitation pulses were selectively applied on the [1–^{13}C]pyruvate peaks to ensure visibility and sufficient signal-to-noise. The liver image shows most pyruvate signal primarily centred around the heptic vein, whereas the kidney image shows most pyruvate signal centred around the renal vein. The current imaging data does not contain information on the metabolic products and only visualized the SABRE-hyperpolarized [1–^{13}C]pyruvate; nevertheless, the CSI approach will be critical in future studies imaging disease models, where the production of metabolites may be strongly modulated. For example, the production of lactate is often greatly increased in the presence of tumors because of the Warburg effect[3,66-70].

Cryogen-free 1.5 T hyperpolarized in vivo spectroscopy

In tandem with the work performed at MGH, experiments were conducted at NC State using a cryogen-free variable-field MRI scanner. The use of a cryogen-free MRI and lower magnetic fields circumvents the need for large amounts of helium, reducing installation and maintenance costs. Examples of D-DNP detected with 1 T permanent magnets have been described [71]. With SABRE, even the combination with portable bedside ("point-of-care") MRI[51,52] becomes imaginable. The variable field of our unique MRI (5 mT - 3 T) assists with the broader translation into clinical settings, as the common clinical fields are between 1.5 - 3 T. Studies closely comparable to those performed on the preclinical 4.7T MGH scanner are shown here. Differences reside in the use of a whole body volume coil instead of surface coils, slightly smaller animals (~200 g *versus* ~250 g), and operation at 1.5 T. The selection of 1.5 T helps to establish direct correlation to more clinical settings often operating at this field. Fig. 5A shows summed spectra of the hyperpolarized pyruvate, along with its downstream metabolic products lactate and alanine, as well as the bicarbonate as minor metabolite and pyruvate-hydrate as minor byproduct. Since the 1.5 T data is acquired using a full-body coil, the signal represents an average across the whole rat, showing lower metabolic activity in comparison to the [1–^{13}C]pyruvate signal from the liver and kidney (which are more metabolically active organs). In addition, shimming the magnetic field over a full body is more challenging than over individual organs, which is reflected in broader spectral features visible in Fig. 5A, in contrast to those from Figs. 3A and C. Despite these challenges hyperpolarized signal is detectable for over one minute, and time-resolved metabolism could be observed as illustrated in Figs. 5B and C—presented in analogy to Fig. 3. Overall, the experiments shown in Fig. 5 indicate the successful combination of low-cost hyperpolarization with low-cost MRI to achieve *in vivo* detection of metabolic transformations, advancing this technology and setting the stage for future developments and biomedical applications.

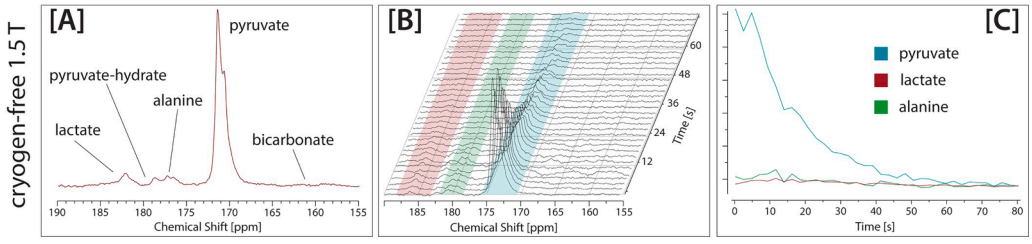

Fig. 5. *In vivo* spectra acquired on one [Wistar, female] rat using a dynamic spectroscopy sequence. [A] Summed spectra of the complete dynamic spectroscopy acquisition. [B] Stack plot of the dynamic spectroscopy acquisition with lactate (red), alanine (green), and pyruvate (blue) integration regions highlighted. [C] Plot of the integrated acquisition for pyruvate, lactate, and alanine using the spectra shown in B. The spectra in this temporal series are acquired with a 20-degree flip angle and a 2 s delay between acquisitions.

Cryogen-free 1.5 T hyperpolarized in vivo spectroscopy using [1–^{13}C] pyruvate hyperpolarized in an ethanol-water mixture followed by catalyst filtration

Although SABRE has seen significant advances as leveraged in the above sections, there are still barriers to clinical translation because of the usage of methanol, and the presence of the iridium catalyst. The SABRE community has put effort into moving towards biocompatibility (*i.e.* a catalyst free, aqueous solution), including developments in water soluble catalysts [40,72–74], heterogenous catalysts[75–77], and dissolution schemes. [65,78,79] However, none of the described methods have established *in vivo* use. In this section, we showcase the first methanol free solution with catalyst filtration of hyperpolarized pyruvate detected *in vivo* employing SABRE. To attain sufficient solubility of [1–^{13}C]pyruvate in ethanol, a 9-to-1 ethanol-water mixture was used, which balances solubility restrictions of both sodium [1–^{13}C]pyruvate and the [Ir(IMes)(COD)Cl] SABRE pre-catalyst. Sodium pyruvate is essentially insoluble in pure ethanol and the SABRE catalyst is insoluble in water. The 9-to-1 ethanol water mixture was found to work well providing sufficient hyperpolarization for *in vivo* detection as described in the following.

First, a 500μL solution of an ethanol and water medium with 6 mM Ir-IMes catalyst, 20 mM dimethyl sulfoxide, and 30 mM [1–^{13}C]pyruvate was prepared. Next, hyperpolarized [1–^{13}C]pyruvate was generated by bubbling parahydrogen at 200 sccm and 150 psi for 60 s at 0.4 μT during active temperature cycling initialized at 0 °C, as previously demonstrated in methanol[45]. The reproducibility was assessed across multiple days and ten samples, resulting in an average polarization of p = 4.5 ± 0.7% on free [1–^{13}C]pyruvate. The polarization achieved in this work is significantly higher than previous reports in ethanolic media [65]. The spectrum with the largest observed polarization on free [1–^{13}C]pyruvate, p = 5.8%, is shown in Fig. 6A.

To further reduce the toxicity of the SABRE sample, we utilized a filtration method for catalyst removal prior to injection. Specifically, we employed commercially available C18 silica cartridges (Waters, SepPak Plus), where the non-polar nature of the column has strong interactions with the non-polar portion of the SABRE catalyst (IMes ligand), whereas the highly polar pyruvate ion remains in the mobile, polar phase. We used mass spectrometry to quantify the efficacy of the filters. Encouragingly, the filters were able to remove > 95% of the iridium from the sample, as summarized in Table 1, with no additional optimization. This corresponds to an average iridium content of 6 ± 2 ppm in the injected solution (1.5 mL total, experiment repeated 3 times). Future optimization of the non-polar filtration phase is expected to reduce the catalyst content further.

To validate the utility of using methanol free solutions with catalyst filtration, we performed an *in vivo* spectroscopic study using the variable field, cryogen free MRI set at 1.5 T as described above. We followed a similar experimental procedure to the pilot SABRE *in vivo* studies presented above. In this procedure, highly polarized [1–^{13}C]pyruvate is first generated in an NMR tube. The tube is then inserted into a Halbach array to ensure adiabaticity during depressurization and ejection into a syringe. We note that magnetic field control in this step is vital to retain the polarization. The syringe, which is prefilled with 1 mL saline, is then quickly transported to the catheterized rat injection line. In contrast to the methods described above, a filter was added to the injection line for catalyst removal, as illustrated in Fig. 6B. Following injection, we employed a temporal pulse sequence using 20° excitation pulses every 2 s to monitor pyruvate resonance signals *in vivo*. The result of the described method is displayed in Fig. 6C, where pyruvate resonance signals were detected for over 30 s. Fig. 6D showcases the summed spectra of the complete temporal series, where production of pyruvate metabolites could be observed.

Table 1
Quantification of SABRE catalyst removal using commercially available C18 silica cartridges.

Sample	Iridium content [ppm]
Blank	1
Unfiltered	256
Filtered	6 ± 2

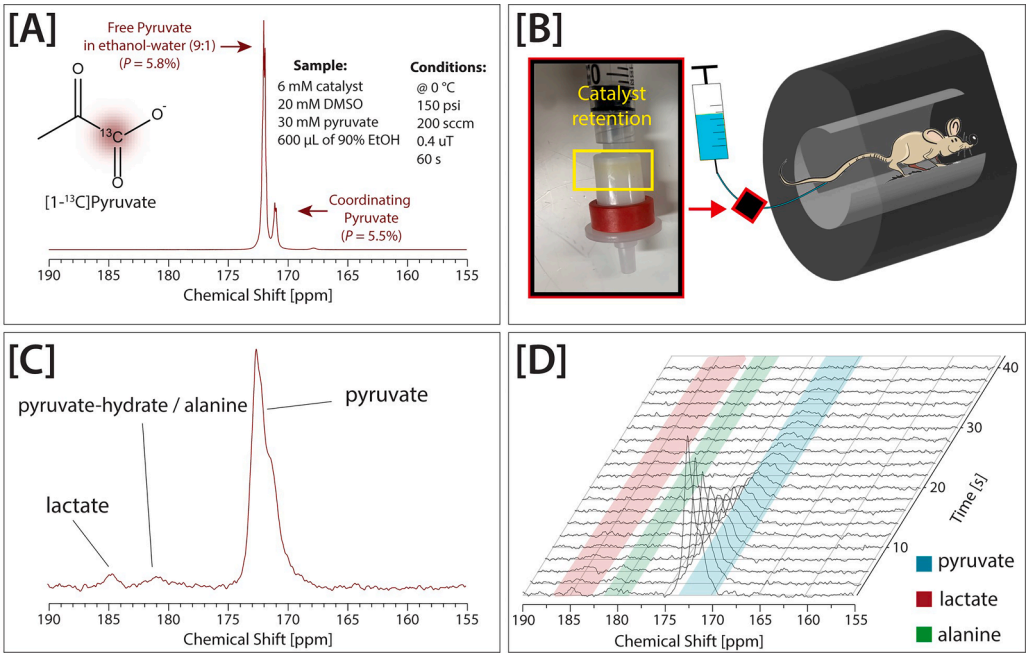

Fig. 6. [A] Hyperpolarized pyruvate generated in an 9:1 ethanol water mixture. [B] Schematic incorporating a C-18 filter into the experimental procedure. [C] Summed and [D] stacked spectra of experimental results from a temporal acquisition using 20° flip angles (TR = 2 s) of hyperpolarized pyruvate, generated in an ethanol-water medium with subsequent catalyst filtration, detected in a healthy Wistar rat.

Conclusion

The first *in vivo* metabolic hyperpolarized MRI experiments were demonstrated using SABRE hyperpolarization chemistry and [1–^{13}C] pyruvate as an exogenous molecular probe. [1-^{13}C]pyruvate is the leading molecular probe because it is a key metabolite that is often dysregulated in many disease states. *In vivo* studies were performed on two different instruments at two different sites to provide multi-site validation of the emerging SABRE technology: a 4.7 T magnet at MGH and a 1.5 T cryogen-free magnet at NC State. We also note that further multi site validation is provided by a group from Freiburg University that was able to provide first *in vivo* data using SABRE-polarized pyruvtate at the same time [80]. Both MRI systems showed good signal-to-noise for the detection of SABRE-hyperpolarized [1–^{13}C]pyruvate and enabled real-time metabolic tracking of the formation of lactate, alanine, and bicarbonate. (The formation of pyruvate-hydrate is also observed.) The presented work is a milestone in the translation of SABRE hyperpolarization chemistry—which has been under development for almost 15 years since inception—to pre-clinical applications focused on biomedical questions.

The presented work includes injections of methanol-water mixtures that still contain hyperpolarization catalyst showing clear conversion of pyruvate to alanine, lactate and bicarbonate. These experiments also enable Chemical Shift Imaging. For ultimate preclinical or clinical translation, methanol and iridium catalyst are not acceptable, therefore we also presented hyperpolarization in ethanol-water mixtures followed by dilution with saline and filtration, while retaining the polarization such that *in vivo* detection was still possible. Yet for widespread use further improvements to the sample processing protocol are still needed.

The facile nature of SABRE hyperpolarization chemistry makes SABRE based technology a good candidate for broader dissemination with the potential to become competitive in the landscape of existing molecular imaging technologies, and medical imaging at large. Specifically, the combination of portable, low-field MRI approaches that otherwise suffer from significant sensitivity limitations could be combined with relatively simple SABRE hyperpolarization chemistry working towards broadly available molecular imaging with the ability to track individual metabolic pathways.

Author contributions

The manuscript was written through contributions of all authors. All authors have given approval to the final version of the manuscript.

Funding sources

This work was supported by the NSF under grants CHE-1904780 and CHE-1905341, and the National Institutes of Health (NIH) under R01EB029829, S10OD021768, and R21GM137227. The content is solely the responsibility of the authors and does not necessarily represent the official views of the NIH. TT also acknowledges funding from the Goodnight foundation. MSR acknowledges the gracious support of the Kiyomi and Ed Baird MGH Research Scholar Award. We also would like to acknowledge the support from NCSU's METRIC providing access to NMR instrumentation. This material is based upon work supported by the U.S. Department of Energy, Office of Biological and Environmental Research (BER) under Award Number(s) DE-SC0023334. Disclaimer: "This report was prepared as an account of work sponsored by an agency of the United States Government. Neither the United States Government nor any agency thereof, nor any of their employees, makes any warranty, express or implied, or assumes any legal liability or responsibility for the accuracy, completeness, or usefulness of any information, apparatus, product, or process disclosed, or represents that its use would not infringe privately owned rights. Reference herein to any specific commercial product, process, or service by trade name, trademark, manufacturer, or otherwise does not necessarily constitute or imply its endorsement, recommendation, or favoring by the United States Government or any agency thereof. The views and opinions of authors expressed herein do not necessarily state or reflect those of the United States Government or any agency.

Declaration of Competing Interest

The authors declare the following financial interests/personal relationships which may be considered as potential competing interests:

PT, CD, TT and MSR are co-founders and equity holders of Vizma Life Sciences (VLS). CD and PT are employees of VLS. EYC is an equity holder of Vizma Life Sciences. The terms of TT's arrangement have been reviewed and approved by NC State University in accordance with its policy on objectivity in research. EYC and BMG hold ownership stakes in XeUS Technologies Ltd. MSR is a founder and equity holder of Hyperfine Inc. All other authors declare that they have no competing interest.

Data availability

Data will be made available on request.

References

[1] J. Eills, D. Budker, S. Cavagnero, E.Y. Chekmenev, S.J. Elliott, S. Jannin, A. Lesage, J. Matysik, T. Meersmann, T. Prisner, J.A. Reimer, H. Yang, Koptyug, I. V. Spin hyperpolarization in modern magnetic resonance, Chem. Rev. (2023), https://doi.org/10.1021/acs.chemrev.2c00534.

[2] S.J. Nelson, J. Kurhanewicz, D.B. Vigneron, P.E.Z. Larson, A.L. Harzstark, M. Ferrone, M. Van Criekinge, J.W. Chang, R. Bok, I. Park, G. Reed, L. Carvajal, E. J. Small, P. Munster, V.K. Weinberg, J.H. Ardenkjaer-Larsen, A.P. Chen, R.E. Hurd, L.I. Odegardstuen, F.J. Robb, J. Tropp, J.A. Murray, Metabolic imaging of patients with prostate cancer using hyperpolarized [1-^{13}C]pyruvate, Sci. Transl. Med. 5 (198) (2013), https://doi.org/10.1126/scitranslmed.3006070.

[3] J. Kurhanewicz, D.B. Vigneron, J.H. Ardenkjaer-Larsen, J.A. Bankson, K. Brindle, C.H. Cunningham, F.A. Gallagher, K.R. Keshari, A. Kjaer, C. Laustsen, D. A. Mankoff, M.E. Merritt, S.J. Nelson, J.M. Pauly, P. Lee, S. Ronen, D.J. Tyler, S. S. Rajan, D.M. Spielman, L. Wald, X. Zhang, C.R. Malloy, R. Rizi, Hyperpolarized ^{13}C MRI: path to clinical translation in oncology, Neoplasia 21 (1) (2019) 1–16, https://doi.org/10.1016/J.NEO.2018.09.006.

[4] Z.J. Wang, M.A. Ohliger, P.E.Z. Larson, J.W. Gordon, R.A. Bok, J. Slater, J. E. Villanueva-Meyer, C.P. Hess, J. Kurhanewicz, D.B. Vigneron, Hyperpolarized ^{13}C MRI: state of the art and future directions, Radiology 291 (2) (2019) 273–284, https://doi.org/10.1148/radiol.2019182391.

[5] J.B. Hövener, A.N. Pravdivtsev, B. Kidd, C.R. Bowers, S. Glöggler, K.V. Kovtunov, M. Plaumann, R. Katz-Brull, K. Buckenmaier, A. Jerschow, F. Reineri, T. Theis, R. V. Shchepin, S. Wagner, P. Bhattacharya, N.M. Zacharias, E.Y. Chekmenev, Parahydrogen-based hyperpolarization for biomedicine, Angew. Chem. Int. Ed 57 (35) (2018) 11140–11162, https://doi.org/10.1002/ANIE.201711842.

[6] K.V. Kovtunov, E.V. Pokochueva, O.G. Salnikov, S.F. Cousin, D. Kurzbach, B. Vuichoud, S. Jannin, E.Y. Chekmenev, B.M. Goodson, D.A. Barskiy, I. V.. Koptyug, H.yperpolarized NMR spectroscopy: D-DNP, PHIP, and SABRE techniques, Chem. Asian J. 13 (15) (2018) 1857–1871, https://doi.org/10.1002/ASIA.201800551.

[7] L.L. Walkup, J.C. Woods, Translational applications of hyperpolarized ^{3}He and ^{129}Xe, NMR Biomed. 27 (12) (2014) 1429–1438, https://doi.org/10.1002/NBM.3151.

[8] J.P. Mugler, T.A. Altes, Hyperpolarized 129Xe MRI of the human lung, J. Magnetic Resonance Imaging 37 (2) (2013) 313–331, https://doi.org/10.1002/JMRI.23844.

[9] J.T. Grist, G.J. Collier, H. Walters, M. Kim, M. Chen, G. Abu Eid, A. Laws, V. Matthews, K. Jacob, S. Cross, A. Eves, M. Durrant, A. McIntyre, R. Thompson, R. F. Schulte, B. Raman, P.A. Robbins, J.M. Wild, E. Fraser, F. Gleeson, Lung abnormalities detected with hyperpolarized ^{129}Xe MRi in patients with long COVID, Radiology 305 (3) (2022) 709–717, https://doi.org/10.1148/radiol.220069.

[10] D.A. Barskiy, A.M. Coffey, P. Nikolaou, D.M. Mikhaylov, B.M. Goodson, R. T. Branca, G.J. Lu, M.G. Shapiro, V.V. Telkki, V.V. Zhivonitko, I.V. Koptyug, O. G. Salnikov, K.V. Kovtunov, V.I. Bukhtiyarov, M.S. Rosen, M.J. Barlow, S. Safavi, I. P. Hall, L. Schröder, E.Y. Chekmenev, NMR hyperpolarization techniques of gases, Chem. - Eur. J. 23 (4) (2017) 725–751, https://doi.org/10.1002/CHEM.201603884.

[11] P. Nikolaou, Boyd.M. Goodson, E.Y. Chekmenev, NMR hyperpolarization techniques for biomedicine, Chem. Eur. J. 21 (8) (2015) 3156–3166, https://doi.org/10.1002/chem.201405253.

[12] K.M. Brindle, K.R. Keshari, Editorial commentary for the special issue: technological developments in hyperpolarized ^{13}C imaging—toward a deeper

understanding of tumor metabolism *in vivo*, Magnetic Resonance Mater. Phys. Biol. Med. 34 (1) (2021) 1–3, https://doi.org/10.1007/s10334-021-00908-1.
[13] J.W. Fletcher, B. Djulbegovic, H.P. Soares, B.A. Siegel, V.J. Lowe, G.H. Lyman, R. E. Coleman, R. Wahl, J.C. Paschold, N. Avril, L.H. Einhorn, W.W. Suh, D. Samson, D. Delbeke, M. Gorman, A.F. Shields, Recommendations on the use of ^{18}F-FDG PET in oncology, J. Nuclear Med. 49 (3) (2008) 480–508, https://doi.org/10.2967/JNUMED.107.047787.
[14] S. Basu, S. Hess, P.E. Nielsen Braad, B.B. Olsen, S. Inglev, P.F. Høilund-Carlsen, The basic principles of FDG-PET/CT imaging, PET Clin. 9 (4) (2014) 355–370, https://doi.org/10.1016/J.CPET.2014.07.006.
[15] C.H. Cunningham, J.Y.C. Lau, A.P. Chen, B.J. Geraghty, W.J. Perks, I. Roifman, G. A. Wright, K.A. Connelly, Hyperpolarized ^{13}C metabolic MRI of the human heart: initial experience, Circ. Res. 119 (11) (2016), https://doi.org/10.1161/CIRCRESAHA.116.309769.
[16] O.J. Rider, A. Apps, J.J.J.J. Miller, J.Y.C. Lau, A.J.M. Lewis, M.A. Peterzan, M. S. Dodd, A.Z. Lau, C. Trumper, F.A. Gallagher, J.T. Grist, K.M. Brindle, S. Neubauer, D.J. Tyler, Noninvasive *in vivo* assessment of cardiac metabolism in the healthy and diabetic human heart using hyperpolarized ^{13}C MRI, Circ. Res. (2020) 725–736, https://doi.org/10.1161/CIRCRESAHA.119.316260.
[17] J.H. Ardenkjær-Larsen, B. Fridlund, A. Gram, G. Hansson, L. Hansson, M.H. Lerche, R. Servin, M. Thaning, K. Golman, Increase in signal-to-noise ratio of >10,000 times in liquid-state NMR, Proc. Natl. Acad. Sci. U S A 100 (18) (2003) 10158–10163, https://doi.org/10.1073/pnas.1733835100.
[18] C.R. Bowers, D.P. Weitekamp, Parahydrogen and synthesis allow dramatically enhanced nuclear alignment, J. Am. Chem. Soc. 109 (18) (1987) 5541–5542, https://doi.org/10.1021/ja00252a049.
[19] C.R. Bowers, D.P. Weitekamp, Transformation of symmetrization order to nuclear spin magnetization by chemical reaction and nuclear magnetic resonance, Phys. Rev. Lett. 57 (21) (1986) 2645–2648, https://doi.org/10.1103/PhysRevLett.57.2645.
[20] Schmidt, A.; Bowers, C.; Buckenmeier, K.; Chekmenev, E.; de Maissin, H.; Eills, J.; Ellermann, F.; Gloggler, S.; Gordon, J.; Knecht, S.; Koptyug, I.; Kuhn, J.; Pravdivtsev, A.; Reineri, F.; Theis, T.; Them, K.; Hövener, J.B. Instrumentation for hydrogenative parahydrogen-based hyperpolarization techniques. *Anal. Chem.* 94 (1), 479–502. https://doi.org/10.1021/acs.analchem.1c04863.
[21] F. Reineri, T. Boi, S. Aime, ParaHydrogen induced polarization of ^{13}C carboxylate resonance in acetate and pyruvate, Nat. Commun. 6 (1) (2015) 1–6, https://doi.org/10.1038/ncomms6858.
[22] E. Cavallari, C. Carrera, S. Aime, F. Reineri, Studies to enhance the hyperpolarization level in PHIP-SAH-Produced ^{13}C-pyruvate, J. Magnetic Resonance 289 (2018) 12–17, https://doi.org/10.1016/j.jmr.2018.01.019.
[23] A. Svyatova, V.P. Kozinenko, N.V. Chukanov, D.B. Burueva, E.Y. Chekmenev, Y. W. Chen, D.W. Hwang, K.V. Kovtunov, I.V.PHIP Koptyug, Hyperpolarized [1-^{13}C] Pyruvate and [1-13C]Acetate esters via PH-INEPt polarization transfer monitored by ^{13}C NMR and MRI, Sci. Rep. 11 (1) (2021) 5646, https://doi.org/10.1038/S41598-021-85136-2.
[24] T. Hune, S. Mamone, H. Schroeder, A.P. Jagtap, S. Sternkopf, G. Stevanato, S. Korchak, C. Fokken, C.A. Müller, A.B. Schmidt, D. Becker, S. Glöggler, Metabolic tumor imaging with rapidly signal-enhanced 1-13C-Pyruvate-D3, ChemPhysChem 24 (2) (2023), e202200615, https://doi.org/10.1002/CPHC.202200615.
[25] G. Stevanato, Y. Ding, S. Mamone, A.P. Jagtap, S. Korchak, S. Glöggler, Real-time pyruvate chemical conversion monitoring enabled by PHIP, J. Am. Chem. Soc. 145 (2022) 15, https://doi.org/10.1021/jacs.2c13198.
[26] R.W. Adams, J.A. Aguilar, K.D. Atkinson, M.J. Cowley, P.I.P. Elliott, S.B. Duckett, G.G.R. Green, I.G. Khazal, J. Lopez-Serrano, D.C. Williamson, Reversible interactions with para-hydrogen enhance NMR sensitivity by polarization transfer, Science (1979) 323 (5922) (2009) 1708–1711, https://doi.org/10.1126/science.1168877.
[27] K.D. Atkinson, M.J. Cowley, S.B. Duckett, P.I.P. Elliott, G.G.R. Green, J. López-Serrano, I.G. Khazal, A.C. Whitwood, Para-hydrogen induced polarization without incorporation of para-hydrogen into the analyte, Inorg. Chem. 48 (2) (2009) 663–670, https://doi.org/10.1021/ic8020029.
[28] K.D. Atkinson, M.J. Cowley, P.I.P. Elliott, S.B. Duckett, G.G.R. Green, J. López-Serrano, A.C. Whitwood, Spontaneous transfer of parahydrogen derived spin order to pyridine at low magnetic field, J. Am. Chem. Soc. 131 (37) (2009) 13362–13368, https://doi.org/10.1021/ja903601p.
[29] P.J. Rayner, S.B. Duckett, Signal amplification by reversible exchange (SABRE): from discovery to diagnosis, Angew. Chem. Int. Ed. 57 (23) (2018) 6742–6753, https://doi.org/10.1002/anie.201710406.
[30] S.S. Roy, K.M. Appleby, E.J. Fear, S.B. Duckett, SABRE-relay: a versatile route to hyperpolarization, J. Phys. Chem. Lett. 9 (5) (2018) 1112–1117, https://doi.org/10.1021/acs.jpclett.7b03026.
[31] W. Iali, P.J. Rayner, S.B. Duckett, Using parahydrogen to hyperpolarize amines, amides, carboxylic acids, alcohols, phosphates, and carbonates, Sci. Adv. 4 (1) (2018), https://doi.org/10.1126/sciadv.aao6250.
[32] A.M. Olaru, M.J. Burns, G.G.R. Green, S.B. Duckett, SABRE hyperpolarisation of vitamin B_3 as a function of pH, Chem. Sci. 8 (3) (2017) 2257–2266, https://doi.org/10.1039/c6sc04043h.
[33] S.S. Roy, P. Norcott, P.J. Rayner, G.G.R. Green, S.B. Duckett, A hyperpolarizable 1 H magnetic resonance probe for signal detection 15 Min after spin polarization storage, Angewandte Chemie 128 (50) (2016) 15871–15874, https://doi.org/10.1002/ange.201609186.
[34] M. Truong, T. Theis, A. Coffey, R. Shchepin, K. Waddell, F. Shi, B. Goodson, W. Warren, E. Chekmenev, ^{15}N hyperpolarization by reversible exchange using SABRE-SHEATH, J. Phys. Chem. C 119 (16) (2015) 8786–8797, https://doi.org/10.1021/acs.jpcc.5b01799.
[35] R.V. Shchepin, D.A. Barskiy, A.M. Coffey, T. Theis, F. Shi, W.S. Warren, B. M. Goodson, E.Y Chekmenev, ^{15}N hyperpolarization of imidazole-$^{15}N_2$ for magnetic resonance pH sensing via SABRE-SHEATH, ACS Sens. 1 (6) (2016) 640–644, https://doi.org/10.1021/acssensors.6b00231.
[36] T. Theis, M.L. Truong, A.M. Coffey, R.V. Shchepin, K.W. Waddell, F. Shi, B. M. Goodson, W.S. Warren, E.Y. Chekmenev, Microtesla SABRE enables 10% nitrogen-15 nuclear spin polarization, J. Am. Chem. Soc. 137 (4) (2015), https://doi.org/10.1021/ja512242d.
[37] Z. Zhou, J. Yu, J.F.P. Colell, R. Laasner, A. Logan, D.A. Barskiy, R.V. Shchepin, E. Y. Chekmenev, V. Blum, W.S. Warren, T. Theis, Long-lived $^{13}C_2$ nuclear spin states hyperpolarized by parahydrogen in reversible exchange at microtesla fields, J. Phys. Chem. Lett. 8 (13) (2017), https://doi.org/10.1021/acs.jpclett.7b00987.
[38] M. Fekete, F. Ahwal, S.B. Duckett, S. B Duckett, S.B. Duckett, Remarkable levels of ^{15}N polarization delivered through SABRE into unlabeled pyridine, pyrazine, or metronidazole enable single scan NMR quantification at the mM level, J. Phys. Chem. B 124 (22) (2020) 4573–4580, https://doi.org/10.1021/acs.jpcb.0c02583.
[39] R.V. Shchepin, J.R. Birchall, N.V. Chukanov, K.V. Kovtunov, I.V. Koptyug, T. Theis, W.S. Warren, J.G. Gelovani, B.M. Goodson, S. Shokouhi, M.S. Rosen, Y.F. Yen, W. Pham, E.Y. Chekmenev, Hyperpolarizing concentrated metronidazole $^{15}NO_2$ group over six chemical bonds with more than 15% polarization and a 20 min lifetime, Chem. - Eur. J. 25 (37) (2019), https://doi.org/10.1002/chem.201901192.
[40] J.F.P. Colell, M. Emondts, A.W.J. Logan, K. Shen, J. Bae, R.V. Shchepin, G.X. Ortiz, P. Spannring, Q. Wang, S.J. Malcolmson, E.Y. Chekmenev, M.C. Feiters, F.P.J. T. Rutjes, B. Blümich, T. Theis, W.S Warren, Direct hyperpolarization of nitrogen-15 in aqueous media with parahydrogen in reversible exchange, J. Am. Chem. Soc. 139 (23) (2017) 7761–7767, https://doi.org/10.1021/jacs.7b00569.
[41] T. Theis, G.X. Ortiz, A.W.J. Logan, K.E. Claytor, Y. Feng, W.P. Huhn, V. Blum, S. J. Malcolmson, E.Y. Chekmenev, Q. Wang, W.S. Warren, Direct and cost-efficient hyperpolarization of long-lived nuclear spin states on universal $^{15}N_2$-diazirine molecular tags, Sci. Adv. 2 (3) (2016), e1501438, https://doi.org/10.1126/sciadv.1501438.
[42] Shchepin, R.; Jaigirdar, L.; Theis, T.; Warren, W.; Goodson, B.; Chekmenev, E. Spin relays enable efficient long-range heteronuclear signal amplification by reversible exchange. *J. Phys. Chem. C* 121 (51), 28425–28434. https://doi.org/10.1021/acs.jpcc.7b11485.
[43] W. Iali, S.S. Roy, B.J. Tickner, F. Ahwal, A.J. Kennerley, S.B. Duckett, Hyperpolarising pyruvate through signal amplification by reversible exchange (SABRE), Angewandte Chemie - Int. Edition 58 (30) (2019) 10271–10275, https://doi.org/10.1002/anie.201905483.
[44] Ben.J. Tickner, O. Semenova, W. Iali, P.J. Rayner, A.C. Whitwood, S.B. Duckett, Optimisation of Pyruvate Hyperpolarisation Using SABRE by tuning the active magnetisation transfer catalyst, Catal Sci. Technol. 10 (5) (2020) 1343–1355, https://doi.org/10.1039/C9CY02498K.
[45] P. Tomhon, M. Abdulmojeed, I. Adelabu, S. Nantogma, M.S.H. Kabir, S. Lehmkuhl, E.Y. Chekmenev, T. Theis, Temperature cycling enables efficient ^{13}C SABRE-SHEATH hyperpolarization and imaging of [1-^{13}C]-Pyruvate, J. Am. Chem. Soc. 144 (1) (2022), https://doi.org/10.1021/jacs.1c09581.
[46] I. Adelabu, P. TomHon, M.S.H. Kabir, S. Nantogma, M. Abdulmojeed, I. Mandzhieva, J. Ettedgui, R.E. Swenson, M.C. Krishna, T. Theis, B.M. Goodson, E. Y. Chekmenev, Order-unity ^{13}C nuclear polarization of [1-^{13}C]pyruvate in seconds and the interplay of water and SABRE enhancement, ChemPhysChem 23 (2) (2022), e202100839, https://doi.org/10.1002/CPHC.202100839.
[47] J.R. Lindale, S.L. Eriksson, C.P.N. Tanner, Z. Zhou, J.F.P. Colell, G. Zhang, J. Bae, E.Y. Chekmenev, T. Theis, W.S. Warren, Unveiling coherently driven hyperpolarization dynamics in signal amplification by reversible exchange, Nat. Commun. 10 (1) (2019), https://doi.org/10.1038/s41467-019-08298-8.
[48] S. Nantogma, S.L. Eriksson, I. Adelabu, I. Mandzhieva, A. Browning, P. TomHon, W.S. Warren, T. Theis, B.M. Goodson, E.Y. Chekmenev, Interplay of near-zero-field dephasing, rephasing, and relaxation dynamics and [1-^{13}C]pyruvate polarization transfer efficiency in pulsed SABRE-SHEATH, J. Phys. Chem. A 126 (48) (2022), https://doi.org/10.1021/acs.jpca.2c07150.
[49] T. Theis, N.M. Ariyasingha, R.V. Shchepin, J.R. Lindale, W.S. Warren, E. Y. Chekmenev, Quasi-resonance signal amplification by reversible exchange, J. Phys. Chem. Lett. 9 (20) (2018), https://doi.org/10.1021/acs.jpclett.8b02669.
[50] N.M. Ariyasingha, J.R. Lindale, S.L. Eriksson, G.P. Clark, T. Theis, R.V. Shchepin, N.V. Chukanov, K.V. Kovtunov, I.V. Koptyug, W.S. Warren, E.Y. Chekmenev, Quasi-Resonance Fluorine-19 Signal Amplification by Reversible Exchange, J. Phys. Chem. Lett. 10 (15) (2019), https://doi.org/10.1021/acs.jpclett.9b01505.
[51] M. Sarracanie, C.D. LaPierre, N. Salameh, D.E.J. Waddington, T. Witzel, M. S. Rosen, Low-cost high-performance MRI, Sci. Rep. 5 (2015) 15177, https://doi.org/10.1038/srep15177.
[52] A. Cho, MRI for all, Science 379 (6634) (2023) 748–751, https://doi.org/10.1126/SCIENCE.ADH2295.
[53] S. Lehmkuhl, M. Suefke, A. Kentner, Y.F. Yen, B. Blümich, M.S. Rosen, S. Appelt, T. Theis, SABRE polarized low field rare-spin spectroscopy, J. Chem. Phys. 152 (18) (2020) 1–9, https://doi.org/10.1063/5.0002412.
[54] A.M. Prabhat, A.L. Crawford, M.H. Mazurek, M.M. Yuen, I.R. Chavva, A. Ward, W. V. Hofmann, N. Timario, S.R. Qualls, J. Helland, C. Wira, G. Sze, M.S. Rosen, W. T. Kimberly, K.N. Sheth, Methodology for low-field, portable magnetic resonance neuroimaging at the bedside, Front. Neurol. 12 (2021) 2191, https://doi.org/10.3389/FNEUR.2021.760321/BIBTEX.
[55] J.E. Iglesias, R. Schleicher, S. Laguna, B. Billot, P. Schaefer, B. McKaig, J. N. Goldstein, K.N. Sheth, M.S. Rosen, W.T. Kimberly, Quantitative brain morphometry of portable low-field-strength MRI using super-resolution machine learning, Radiology (2022), https://doi.org/10.1148/radiol.220522.

[56] M.J. Cowley, R.W. Adams, K.D. Atkinson, M.C.R. Cockett, S.B. Duckett, G.G. R. Green, J.A.B. Lohman, R. Kerssebaum, D. Kilgour, R.E. Mewis, Iridium N-heterocyclic carbene complexes as efficient catalysts for magnetization transfer from para-hydrogen, J. Am. Chem. Soc. 133 (16) (2011) 6134–6137, https://doi.org/10.1021/ja200299u.

[57] L.D. Vazquez-Serrano, B.T. Owens, J.M. Buriak, The search for new hydrogenation catalyst motifs based on N-heterocyclic Carbene ligands, Inorg. Chim. Acta 359 (9) (2006) 2786–2797, https://doi.org/10.1016/j.ica.2005.10.049.

[58] S.J. Kohler, Y. Yen, J. Wolber, A.P. Chen, M.J. Albers, R. Bok, V. Zhang, J. Tropp, S. Nelson, D.B. Vigneron, J. Kurhanewicz, R.E. Hurd, *In Vivo* 13 Carbon metabolic imaging at 3T with hyperpolarized ^{13}C-1-pyruvate, Magn. Reson. Med. 58 (1) (2007) 65–69, https://doi.org/10.1002/mrm.21253.

[59] J.M. Park, L.D. Recht, S. Josan, M. Merchant, T. Jang, Y.F. Yen, R.E. Hurd, D. M. Spielman, D. Mayer, Metabolic response of glioma to dichloroacetate measured *in vivo* by hyperpolarized ^{13}C magnetic resonance spectroscopic imaging, Neuro Oncol. 15 (4) (2013), https://doi.org/10.1093/neuonc/nos319.

[60] V. Hyppönen, P. Stenroos, R. Nivajärvi, J.H. Ardenkjær-Larsen, O. Gröhn, J. Paasonen, M.I. Kettunen, Metabolism of hyperpolarised [1-^{13}C]pyruvate in awake and anaesthetised rat brains, NMR Biomed. 35 (2) (2022), https://doi.org/10.1002/nbm.4635.

[61] Y.F. Yen, P.Le Roux, D. Mayer, R. King, D. Spielman, J. Tropp, K.B. Pauly, A. Pfefferbaum, S. Vasanawala, R Hurd, T2 relaxation times of ^{13}C metabolites in a rat hepatocellular carcinoma model measured *in vivo* using ^{13}C-MRS of hyperpolarized [1-^{13}C]pyruvate, NMR Biomed. 23 (4) (2010), https://doi.org/10.1002/nbm.1481.

[62] X. Liu, S. Tang, C. Mu, H. Qin, D. Cui, Y.C. Lai, A.M. Riselli, R. Delos Santos, L. Carvajal, D. Gebrezgiabhier, R.A. Bok, H.Y. Chen, R.R. Flavell, J.W. Gordon, D. B. Vigneron, J. Kurhanewicz, P.E.Z Larson, Development of specialized magnetic resonance acquisition techniques for human hyperpolarized [^{13}C,^{15}N$_2$]Urea + [1-^{13}C]pyruvate simultaneous perfusion and metabolic imaging, Magn. Reson. Med. 88 (3) (2022) 1039–1054, https://doi.org/10.1002/mrm.29266.

[63] Y.L. Dorokhov, A.V. Shindyapina, E.V. Sheshukova, T.V. Komarova, Metabolic methanol: molecular pathways and physiological roles, Physiol. Rev. 95 (2) (2015) 603–644, https://doi.org/10.1152/physrev.00034.2014.

[64] Skrzydlewska, E. Toxicological and metabolic consequences of methanol poisoning. *10.1080/713857189* 2008, 13 (4), 277–293. https://doi.org/10.1080/713857189.

[65] A.B. Schmidt, H. De Maissin, I. Adelabu, S. Nantogma, J. Ettedgui, P. Tomhon, B. M. Goodson, T. Theis, E.Y. Chekmenev, Catalyst-free aqueous hyperpolarized [1-^{13}C]pyruvate obtained by *re*-dissolution signal amplification by reversible exchange, ACS Sens. 7 (11) (2022) 3430–3439, https://doi.org/10.1021/acssensors.2c01715.

[66] C. Hundshammer, M. Braeuer, C.A. Müller, A.E. Hansen, M. Schillmaier, S. Düwel, B. Feuerecker, S.J. Glaser, A. Haase, W. Weichert, K. Steiger, J. Cabello, F. Schilling, J.B. Hövener, A. Kjær, S.G. Nekolla, M. Schwaiger, Simultaneous characterization of tumor cellularity and the warburg effect with PET, MRI and hyperpolarized ^{13}C-MRSI, Theranostics 8 (17) (2018) 4765–4780, https://doi.org/10.7150/THNO.25162.

[67] B.T. Scroggins, M. Matsuo, A.O. White, K. Saito, J.P. Munasinghe, C. Sourbier, K. Yamamoto, V. Diaz, Y. Takakusagi, K. Ichikawa, J.B. Mitchell, M.C. Krishna, D. E. Citrin, Hyperpolarized [1-^{13}C]-pyruvate magnetic resonance spectroscopic imaging of prostate cancer *in vivo* predicts efficacy of targeting the warburg effect, Clin. Cancer Res. 24 (13) (2018) 3137–3148, https://doi.org/10.1158/1078-0432.CCR-17-1957.

[68] M.V. Liberti, J.W. Locasale, The Warburg effect: how does it benefit cancer cells? Trends Biochem. Sci. 41 (3) (2016) 211–218, https://doi.org/10.1016/j.tibs.2015.12.001.

[69] O. Warburg, Über Den Stoffwechsel Der Carcinomzelle, Naturwissenschaften 12 (50) (1924), https://doi.org/10.1007/BF01504608.

[70] M.J. Albers, R. Bok, A.P. Chen, C.H. Cunningham, M.L. Zierhut, V.Y. Zhang, S. J. Kohler, J. Tropp, R.E. Hurd, Y.F.F. Yen, S.J. Nelson, D.B. Vigneron, J. Kurhanewicz, Hyperpolarized ^{13}C lactate, pyruvate, and alanine: noninvasive biomarkers for prostate cancer detection and grading, Cancer Res. 68 (20) (2008) 8607–8615, https://doi.org/10.1158/0008-5472.CAN-08-0749.

[71] S.S. Tee, V. DiGialleonardo, R. Eskandari, S. Jeong, K.L. Granlund, V. Miloushev, A. J. Poot, S. Truong, J.A. Alvarez, H.N. Aldeborgh, K.R. Keshari, Sampling hyperpolarized molecules utilizing a 1 tesla permanent magnetic field, Sci. Rep. 6 (2016) 32846, https://doi.org/10.1038/srep32846. http://www.nature.com/articles/srep32846#supplementary-information.

[72] M.L. Truong, F. Shi, P. He, B. Yuan, K.N. Plunkett, A.M. Coffey, R.V. Shchepin, D. A. Barskiy, K.V. Kovtunov, I.V. Koptyug, K.W. Waddell, B.M. Goodson, E. Y Chekmenev, Irreversible catalyst activation enables hyperpolarization and water solubility for NMR signal amplification by reversible exchange, J. Phys. Chem. B 118 (48) (2014) 13882–13889, https://doi.org/10.1021/jp510825b.

[73] F. Shi, P. He, Q.A. Best, K.A. Groome, M.L. Truong, A.M. Coffey, G. Zimay, R. V. Shchepin, K.W. Waddell, E.Y. Chekmenev, B.M Goodson, Aqueous NMR signal enhancement by reversible exchange in a single step using water-soluble catalysts, J. Phys. Chem. C 120 (22) (2016) 12149–12156, https://doi.org/10.1021/acs.jpcc.6b04484.

[74] M. Fekete, C. Gibard, G.J. Dear, G.G.R. Green, A.J.J. Hooper, A.D. Roberts, F. Cisnetti, S.B. Duckett, Utilisation of water soluble iridium catalysts for signal amplification by reversible exchange, Dalton Trans. 44 (17) (2015) 7870–7880, https://doi.org/10.1039/c5dt00311c.

[75] K.V. Kovtunov, L.M. Kovtunova, M.E. Gemeinhardt, A.V. Bukhtiyarov, J. Gesiorski, V.I. Bukhtiyarov, E.Y. Chekmenev, I.V. Koptyug, B.M. Goodson, Heterogeneous Microtesla SABRE enhancement of ^{15}N NMR signals, Angew. Chem. Int. Ed. 56 (35) (2017), https://doi.org/10.1002/anie.201705014.

[76] F. Shi, A.M. Coffey, K.W. Waddell, E.Y. Chekmenev, B.M. Goodson, Heterogeneous solution NMR signal amplification by reversible exchange, Angewandte Chemie - Int. Edition 53 (29) (2014) 7495–7498, https://doi.org/10.1002/anie.201403135.

[77] D.B. Burueva, L.M. Kovtunova, V.I. Bukhtiyarov, K.V. Kovtunov, I.V. Koptyug, Single-site heterogeneous catalysts: from synthesis to NMR signal enhancement, Chem. - A Eur. J. 25 (6) (2019) 1420–1431, https://doi.org/10.1002/CHEM.201803515.

[78] B.E. Kidd, J.L. Gesiorski, M.E. Gemeinhardt, R.V. Shchepin, K.V. Kovtunov, I. V. Koptyug, E.Y. Chekmenev, B.M. Goodson, Facile removal of homogeneous SABRE catalysts for purifying hyperpolarized metronidazole, a potential hypoxia sensor, J. Phys. Chem. C 122 (29) (2018) 16848–16852, https://doi.org/10.1021/acs.jpcc.8b05758.

[79] A. Manoharan, P.J. Rayner, W. Iali, M.J. Burns, V.H. Perry, S.B. Duckett, Achieving biocompatible SABRE: an invitro cytotoxicity study, ChemMedChem 13 (4) (2018) 352–359, https://doi.org/10.1002/CMDC.201700725.

[80] H. de Maissin, P. R. Gro.., O. Mohiuddin, M. Weigt, L. Nagel, M. Herzog, Z. Wang, R. Willing, W. Reichardt, M. Pichotka, L. He.., T. Reinheckel, H.J. Jessen, R. Zeiser, M. Bock, D. von Elverfeldt, M. Zaitsev, S. Korchak, S. Gl..ggler, J.-B. H..vener, E.Y. Chekmenev, F. Schilling, S. Knecht, A.B. Schmidt, In vivo metabolic imaging of [1-13C]pyruvate-d3 hyperpolarized by reversible exchange With parahydrogen, Angew. Chem. Int. Ed. 2023 e202306654.